

# Simultaneous Detection of LSD and FMD in Cattle Using Ensemble Deep Learning

Nazibul Basar Ayon<sup>1</sup>, Abdul Hasib<sup>\*2</sup>, Md. Faishal Ahmed<sup>2</sup>, Md. Sadiqur Rahman<sup>1</sup>, Kamrul Islam<sup>1</sup>, T. M. Mehrab Hasan<sup>2</sup>, and A. S. M. Ahsanul Sarkar Akib<sup>3</sup>

<sup>1</sup> Department of Computer Science and Engineering,  
Bangladesh University of Business and Technology

[nbasherayon001@gmail.com](mailto:nbasherayon001@gmail.com), [sadiqurrhaman199@gmail.com](mailto:sadiqurrhaman199@gmail.com), [kamruliit78@gmail.com](mailto:kamruliit78@gmail.com)

<sup>2</sup> Department of Internet of Things and Robotics Engineering,  
University of Frontier Technology, Bangladesh  
[sm.abdulhasib.bd@gmail.com](mailto:sm.abdulhasib.bd@gmail.com), [faishalahmed003@gmail.com](mailto:faishalahmed003@gmail.com),  
[mehrabratul210524@gmail.com](mailto:mehrabratul210524@gmail.com)

<sup>3</sup> Robo Tech Valley, Dhaka, Bangladesh  
[ahsanulakib@gmail.com](mailto:ahsanulakib@gmail.com)

**Abstract.** Lumpy Skin Disease (LSD) and Foot-and-Mouth Disease (FMD) are highly contagious viral diseases affecting cattle, causing significant economic losses and welfare challenges. Their visual diagnosis is complicated by significant symptom overlap with each other and with benign conditions like insect bites or chemical burns, hindering timely control measures. Leveraging a comprehensive dataset of 10,516 expert-annotated images from 18 farms across India, Brazil, and the USA, this study presents a novel Ensemble Deep Learning framework integrating VGG16, ResNet50, and InceptionV3 with optimized weighted averaging for simultaneous LSD and FMD detection. The model achieves a state-of-the-art accuracy of 98.2%, with macro-averaged precision of 98.2%, recall of 98.1%, F1-score of 98.1%, and an AUC-ROC of 99.5%. This approach uniquely addresses the critical challenge of symptom overlap in multi-disease detection, enabling early, precise, and automated diagnosis. This tool has the potential to enhance disease management, support global agricultural sustainability, and is designed for future deployment in resource-limited settings.

**Keywords:** Diabetic Retinopathy, Deep Learning, Multi-Modal, Temporal Modeling, Interpretability

## 1 Introduction

Lumpy Skin Disease (LSD) and Foot-and-Mouth Disease (FMD) rank among the most economically and socially devastating viral diseases impacting the global cattle industry, threatening food security, farmer livelihoods, and international trade. LSD, caused by the Lumpy Skin Disease Virus (LSDV), manifests through fever, characteristic skin nodules, emaciation, and enlarged lymph nodes, leading

to substantial reductions in milk yield (up to 40% in severe cases), hide quality deterioration, and occasional mortality [1]. FMD, driven by the Foot-and-Mouth Disease Virus (FMDV), affects cloven-hoofed animals with symptoms including fever, vesicles, and ulcers on the feet and mouth, resulting in severe productivity losses and stringent trade restrictions that can cost billions annually. The World Organisation for Animal Health (OIE) reports that FMD affects over 70 countries, while LSD has spread to new regions, exacerbating global agricultural challenges. The diagnostic complexity arises from symptom overlap with non-viral conditions, such as LSD lesions resembling insect bites or FMD ulcers mimicking chemical burns, leading to misdiagnosis rates as high as 20% [2]. These diagnostic hurdles amplify disease spread, particularly in resource-constrained regions, underscoring the urgent need for advanced, automated diagnostic solutions to enable rapid and accurate intervention.

Deep learning advances enable CNN-based agricultural disease detection, but existing studies focus on single diseases or achieve limited multi-disease success. MobileNetV2 attained 95% LSD accuracy[3], VGG16 showed similar LSD performance but omitted FMD, and MobileNetV3 reached 96.5% LSD accuracy without addressing FMD[4]. EfficientNet approaches also overlooked FMD. Multi-disease efforts (including LSD and FMD) achieved only 95% accuracy due to small datasets and limited validation[5], highlighting gaps in dataset scale, simultaneous detection, and symptom overlap handling. This study introduces a novel ensemble framework (VGG16, ResNet50, InceptionV3 with 0.3/0.3/0.4 weights) for simultaneous LSD and FMD detection. It utilizes 10,516 expert-annotated images from 18 farms across India, Brazil, and the USA, featuring diverse cattle breeds (e.g., Holstein, Zebu) with GPS-tracked provenance and veterinary certifications (publicly available). Key contributions:

1. Novel ensemble framework addressing LSD/FMD symptom overlap
2. Large-scale public dataset with expert annotations and provenance
3. High-performance model enabling precise early diagnosis to reduce economic losses

Unlike existing studies that focused on single-disease detection or achieved limited accuracy in multi-disease contexts, this work introduces a dual-disease ensemble model with a large-scale, expert-certified dataset.

## 2 Literature Review

LSD and FMD are highly contagious viral diseases that severely impact the global cattle industry, causing economic losses through reduced productivity, trade restrictions, and compromised animal welfare [7]. Effective disease control depends heavily on prompt and accurate diagnosis, particularly in resource-constrained regions where veterinary expertise is limited[8]. Deep learning methods, notably CNNs, have proven effective in facilitating automated analysis of medical images for disease detection, offering rapid and scalable diagnostic solutions[9].

Recent studies have advanced LSD detection using deep learning. Chamirti et al. [10] evaluated pretrained models like VGG16 and MobileNetV2 for early LSD detection, achieving high accuracy through data augmentation and balancing. AlZubi [11] employed CNNs to classify LSD and non-LSD images, using metrics like accuracy and confusion matrices to assess performance. A novel CNN architecture achieved 96% accuracy with MobileNetV2 for LSD diagnosis in dairy cows [4]. Muhammad et al. [3] optimized MobileNetV2 with RMSProp, reporting 95% accuracy on LSD-affected cattle images. A customized CBAM-DenseNet-attention model achieved 99.11% accuracy on an augmented dataset, highlighting the potential of attention mechanisms [12]. Another study used InceptionV3 with SVM for LSD classification, achieving 84% accuracy but suggesting advanced models like Vision Transformers for improvement [13].

FMD detection using deep learning is less explored but shows significant potential. Phulu et al. [14] developed a hybrid system combining Random Forest and MobileNetV2, achieving 90.62% and 91.1% accuracies, respectively, by integrating ontological data with image classification. This approach underscores the value of hybrid models for early FMD detection in cattle.

Simultaneous detection of LSD and FMD is challenging due to symptom overlap, which often reduces model accuracy. A study classified cattle skin diseases, including LSD and FMD, using deep learning models, selecting the best performer based on accuracy and precision metrics [15, 18]. Another effort utilized CNN architectures like InceptionV3 and VGG16 to detect FMD, LSD, and other diseases, emphasizing early diagnosis [5]. These studies highlight the need for robust models to address overlapping symptoms in multi-disease scenarios. Understanding LSD and FMD epidemiology and management informs detection strategies. Kim et al. assessed acute phase proteins following simultaneous FMD and LSD vaccination, revealing immune response differences that aid disease management. Mackereth et al. [17] quantified surveillance sensitivity for LSD and FMD in Western Australia, reporting detection probabilities of 0.37 and 0.49, respectively, using scenario tree methodology. A study in Thailand used path analysis to explore farmers' knowledge, attitudes, and practices regarding LSD, identifying gaps in control measures. In Bangladesh, research on LSD's clinical presentation and treatment efficacy highlighted higher susceptibility in local breeds and young cattle.

Single-disease detection achieves high accuracy (99.11% LSD, 91.1% FMD), but multi-disease systems face symptom overlap challenges, reducing performance (approx. 95%; Table 1). This study bridges the gap via an ensemble framework (VGG16, ResNet50, InceptionV3) with weighted averaging (0.3, 0.3, 0.4) and temperature scaling ( $T = 0.8$ ), enhancing simultaneous LSD and FMD detection for precise veterinary diagnostics and sustainable livestock management.

Table 1: Comparison of Deep Learning Approaches for LSD and FMD Detection

Study	Model	Disease	Accuracy
Chamirti et al. [10]	VGG16, MobileNetV2	LSD	High (not specified)
AlZubi [11]	CNN	LSD	86.54%
Saha [4]	MobileNetV2	LSD	96%
Muhammad et al. [3]	MobileNetV2	LSD	95%
Mujahid et al. [12]	DenseNet	LSD	99.11%
Alam et al. [13]	InceptionV3 + SVM	LSD	84%
Phulu et al. [14]	Random Forest, MobileNetV2	FMD	90.62%, 91.1%
Maganti et al. [15]	Deep Learning Models	LSD, FMD	Not specified
Rony et al. [5]	InceptionV3, VGG16	LSD, FMD	95%

### 3 Methodology

The methodology employs a structured pipeline, illustrated in Figure 1. Three convolutional neural networks—VGG16, ResNet50, and InceptionV3—are trained for a six-class classification task[6]. These models are combined into a weighted ensemble, followed by calibration to optimize prediction reliability.

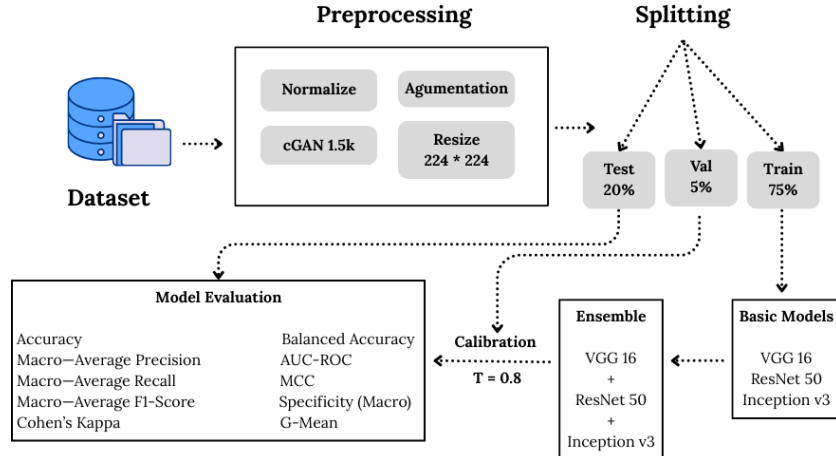


Fig. 1: Methodology flowchart.

#### 3.1 Dataset Description & Data Acquisition

The dataset comprises 10,516 high-resolution images collected from 18 farms across India, Brazil, and the USA, capturing diverse cattle breeds (including Holstein and Zebu) and disease manifestations. Images are categorized into six medically distinct classes: **fmd-foot** (FMD foot lesions characterized by blisters and erosions), **fmd-mouth** (FMD oral lesions including ulcers and excessive

salivation), **healthy-foot** (normal cattle feet free of lesions), **healthy-mouth** (normal oral mucosa without inflammation), **healthy-skin** (normal cattle skin without nodules or scabs), and **lsd-skin** (LSD skin lesions featuring nodules and scabs). Metadata, including GPS coordinates, timestamps, cattle breed, age, and veterinarian-confirmed disease status, are stored in a structured JSON format to ensure full traceability and reproducibility. This rigorous provenance tracking is a key contribution of the dataset. Table 2 details the class distribution, showing both real and synthetic data across training, testing, and validation sets. To address class imbalance in **fmd-foot**, **fmd-mouth**, and **lsd-skin**, 1,500 synthetic images (500 per class) were generated using a conditional Generative Adversarial Network (cGAN).

Table 2: Dataset Composition and Distribution

Class	Training			Testing	Validation	Total
	Real	Synthetic	Total			
<b>fmd-foot</b>	1,050	500	1,550	388	50	1,988
<b>fmd-mouth</b>	1,050	500	1,550	388	50	1,988
<b>healthy-foot</b>	1,550	0	1,550	388	50	1,988
<b>healthy-mouth</b>	1,550	0	1,550	388	50	1,988
<b>healthy-skin</b>	1,000	0	1,000	250	32	1,282
<b>lsd-skin</b>	500	500	1,000	250	32	1,282
<b>Total</b>	<b>6,700</b>	<b>1,500</b>	<b>8,200</b>	<b>2,052</b>	<b>264</b>	<b>10,516</b>

Images were captured with 12 MP RGB cameras (300 DPI) under mixed lighting: natural daylight (5000–6500K) and artificial (3200K). The protocol targeted early/advanced lesions from multiple angles (dorsal/lateral) to enhance features. Metadata (GPS, timestamps, breed, age, vet-confirmed status) are stored in JSON for traceability. Reliability measures include: provenance tracking (GPS/vet IDs), SHA-256 deduplication, quality control (PSNR >22 dB; non-bovine removal via Canny edge detection + veterinary review), and veterinarian-annotated validation (264 images, XML: lesion morphology/class labels[16]). Publicly accessible via repositories (e.g., Zenodo DOI) for reproducibility.

### 3.2 Data Preprocessing

The preprocessing pipeline (Algorithm 1) ensures dataset compatibility and addresses class imbalance in **fmd-foot**, **fmd-mouth**, and **lsd-skin**. Raw images ( $N = 10,516$ ) are resized to  $224 \times 224$  pixels using bilinear interpolation for model input compatibility, then shuffled via Fisher-Yates algorithm to prevent batch bias.

Augmentation applies real-world variations using: rotation ( $\theta_r \in [-35^\circ, 35^\circ]$ ), width/height shifts ( $s_w, s_h \in [0, 0.3]$ ), zoom ( $z \in [0.7, 1.3]$ ), brightness adjustment ( $b \in [0.6, 1.4]$ ), and channel shifts ( $c \in [0, 60.0]$ ), with nearest-neighbor boundary filling implemented via `ImageDataGenerator` parameters. Class imbalance is addressed by generating 1,500 synthetic images ( $\sim 500/\text{class}$ ) using

a conditional GAN with: generator ( $128 \times 128$  latent space, 4 upsampling layers (64-512 filters), batch normalization, LeakyReLU (slope 0.2); discriminator (5 conv layers (32-256 filters), batch normalization, LeakyReLU (slope 0.2), sigmoid output). The cGAN trains for 500 epochs (batch size 32, LR 0.0002) using adversarial loss:

$$\min_G \max_D V(D, G) = \mathbb{E}_{x \sim p_{\text{data}}(x)} [\log D(x|y)] + \mathbb{E}_{z \sim p_z(z)} [\log(1 - D(G(z|y)))] \quad (1)$$

Synthetic images undergo veterinary validation for anatomical accuracy (lesion morphology/color consistency) before resizing to  $224 \times 224$  and normalization to  $[0,1]$ .

---

**Algorithm 1** Data Preprocessing Pipeline

---

**Input:** Raw image set  $D = \{I_1, \dots, I_N\}$ ,  $N = 10,516$   
**Output:** Preprocessed set  $D'$

```

1:  $D' \leftarrow \emptyset$ 
2: for each  $I \in D$  do
3:    $I \leftarrow \text{Resize}(I, 224 \times 224)$                                  $\triangleright$  Bilinear interpolation
4:    $D' \leftarrow D' \cup \{I\}$ 
5: end for
6:  $D' \leftarrow \text{Shuffle}(D', \text{Fisher-Yates})$                                  $\triangleright$  Randomize order
7:  $A \leftarrow \text{SetAugmentation}(\theta_r \in [-35^\circ, 35^\circ], s_w \in [0, 0.3], s_h \in [0, 0.3], z \in [0.7, 1.3], b \in [0.6, 1.4], c \in [0, 60.0])$ 
8: for each  $I \in D'$  do
9:    $I \leftarrow \text{Augment}(I, A, \text{fill} = \text{nearest})$                                  $\triangleright$  Apply transformations
10: end for
11:  $G \leftarrow \text{InitializeCGAN}(z \sim \mathcal{N}(0, 1), \text{dim} = 128 \times 128, \text{layers} = 4, \text{LeakyReLU} = 0.2)$ 
12:  $S \leftarrow \text{GenerateImages}(G, N_s = 1,500, \text{classes} = \{\text{fmd-foot}, \text{fmd-mouth}, \text{lsd-skin}\})$ 
13:  $S \leftarrow \text{Validate}(S, \text{anatomical-accuracy})$                                  $\triangleright$  Veterinary review
14:  $S \leftarrow \text{Resize}(S, 224 \times 224)$                                  $\triangleright$  Bilinear interpolation
15:  $D' \leftarrow D' \cup S$ 
16:  $D' \leftarrow \text{Normalize}(D', [0, 1])$                                  $\triangleright$  Pixel scaling
17: return  $D'$ 

```

---

### 3.3 Individual Model Architectures

Three models—VGG16, ResNet50, and InceptionV3, all Convolutional Neural Networks (CNNs)—are fine-tuned for six-class classification using pretrained ImageNet weights, with configurations detailed in Table 3. Each model outputs a six-class softmax probability distribution.

**VGG16** (19 layers, 138M parameters) consists of 13 convolutional layers ( $3 \times 3$  filters, 64-512 filters), 5 max-pooling layers ( $2 \times 2$ , stride 2), along with three dense layers, formalized as:

$$\text{VGG16}(x) = \text{FC}(\text{MaxPool}(\text{Conv}_{3 \times 3}^n(x))), \quad n = 13 \quad (2)$$

The last 18 layers are fine-tuned to capture disease-specific features with AdamW optimization ( $\text{lr}=0.0001$ ,  $\beta_1 = 0.9$ ,  $\beta_2 = 0.999$ ) and L2 decay (0.01).

**ResNet50** (50 layers, 25.6M parameters) employs residual blocks with skip connections:

$$y = F(x, \{W_i\}) + x \quad (3)$$

Table 3: Model Configurations for Fine-Tuning

Model	Total Layers	Fine-Tuned Layers	Optimizer Parameters	Regularization
VGG16	19	Last 18	AdamW lr=0.0001 $\beta_1 = 0.9$ $\beta_2 = 0.999$ SGD	L2 decay (0.01)
ResNet50	50	Last 15	lr=0.005 momentum=0.9 SGD	Stochastic Depth (0.2)
InceptionV3	48	Last 12	lr=0.005 momentum=0.9	Label Smoothing ( $\epsilon = 0.1$ )

Every block is made up of three convolutional layers ( $1 \times 1$ ,  $3 \times 3$ ,  $1 \times 1$ ). The last 15 layers are fine-tuned using SGD (lr=0.005, momentum=0.9) with Stochastic Depth regularization (drop probability=0.2).

**InceptionV3** (48 layers, 23.9M parameters) utilizes inception modules for multi-scale feature extraction:

$$\text{InceptionV3}(x) = \text{Concat}(\text{Conv}_{1 \times 1}(x), \text{Conv}_{3 \times 3}(x), \text{Conv}_{5 \times 5}(x), \text{Pool}(x)) \quad (4)$$

The last 12 layers are fine-tuned with SGD (lr=0.005, momentum=0.9) and label smoothing ( $\epsilon = 0.1$ ).

### 3.4 Individual Model Training

Training is conducted on two NVIDIA A100 GPUs (40 GB VRAM) for approximately 100 hours using Algorithm 2. Training optimization is guided by the categorical cross-entropy loss:

$$L = - \sum_{c=1}^6 y_c \log(p_c) \quad (5)$$

Optimization follows model-specific schemes: VGG16 uses AdamW:

$$\theta_{t+1} = \theta_t - \eta \cdot \frac{\hat{m}_t}{\sqrt{\hat{v}_t} + \epsilon} - \eta \lambda \theta_t \quad (6)$$

( $\eta = 0.0001$ ,  $\epsilon = 10^{-8}$ ,  $\lambda = 0.01$ ,  $\beta_1 = 0.9$ ,  $\beta_2 = 0.999$ ), while ResNet50 and InceptionV3 use SGD:

$$\theta_{t+1} = \theta_t - \eta \nabla L + \eta \mu (\theta_t - \theta_{t-1}) \quad (7)$$

( $\eta = 0.005$ ,  $\mu = 0.9$ ). Three callbacks are implemented: ReduceLROnPlateau (factor=0.2, patience=10 epochs), ModelCheckpoint (saves best validation loss), and EarlyStopping (patience=20 epochs).

**Algorithm 2** Individual Model Training

---

**Input:** Preprocessed set  $D'$ , model  $M$   
**Output:** Trained model  $M'$

- 1:  $M \leftarrow \text{Initialize}(M, \text{pretrained-weights})$
- 2:  $L \leftarrow \text{SetLoss}(\text{Equation 5})$
- 3:  $\theta \leftarrow \text{UnfreezeLayers}(\theta, \text{Table 3})$
- 4:  $O \leftarrow \text{SetOptimizer}(\text{Table 3})$
- 5:  $R \leftarrow \text{SetRegularization}(\text{Table 3})$
- 6: **for**  $e = 1$  to  $200$  **do**
- 7:    $B \leftarrow \text{SampleMiniBatch}(D', \text{size} = 32)$
- 8:    $\nabla L \leftarrow \text{ComputeGradients}(B, M, L)$
- 9:    $\theta \leftarrow \text{UpdateWeights}(\theta, \nabla L, O, \text{Equation 6 or 7})$
- 10:    $L_v \leftarrow \text{ComputeValidationLoss}(V, M)$
- 11:   **if**  $L_v$  plateaus for 20 epochs **then**
- 12:      $\text{StopTraining}()$
- 13:   **end if**
- 14:    $\eta \leftarrow \text{ReduceLROnPlateau}(\eta, \text{factor} = 0.2, \text{patience} = 10)$
- 15:    $M' \leftarrow \text{SaveBestModel}(M, L_v)$
- 16: **end for**
- 17: **return**  $M'$

---

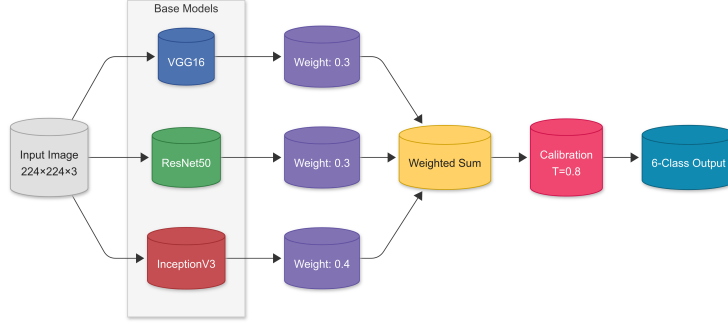


Fig. 2: Ensemble architecture integrating base model predictions.

### 3.5 Ensemble Model and Training

The ensemble architecture (Figure 2) integrates predictions from VGG16, ResNet50, and InceptionV3 using a weighted average:

$$P = w_1 P_{\text{VGG16}} + w_2 P_{\text{ResNet50}} + w_3 P_{\text{InceptionV3}} \quad (8)$$

with weights  $w_1 = 0.30$ ,  $w_2 = 0.30$ , and  $w_3 = 0.40$  optimized through grid search over  $[0.1, 0.5]$  in 0.05 increments, constrained by  $\sum w_i = 1$ . This combination maximized validation accuracy.

Probability calibration enhances reliability using temperature scaling ( $T = 0.8$ ):

$$p'_c = \frac{\exp(z_c/T)}{\sum_{j=1}^6 \exp(z_j/T)} \quad (9)$$

where  $z_c$  represents class logits, sharpening confidence estimates while maintaining class ranking.

### 3.6 Evaluation Preparation

Performance is evaluated across the six-class classification task using comprehensive metrics: accuracy (overall correctness), macro precision (class-average positive predictive value), macro recall (class-average sensitivity), macro F1-score (harmonic average of precision and recall), class-average (Area Under the Receiver Operating Characteristic Curve) AUC-ROC (separation capability), Cohen’s Kappa[20] (chance-adjusted agreement), balanced accuracy (average recall), Matthews Correlation Coefficient - MCC[21] (classification correlation), macro specificity (class-average true negative rate), and G-Mean (geometric mean of recall and specificity).

Standard metrics use conventional definitions: accuracy as  $\frac{TP+TN}{TP+TN+FP+FN}$ , macro precision as  $\frac{1}{6} \sum_{c=1}^6 \frac{TP_c}{TP_c+FP_c}$ , macro recall as  $\frac{1}{6} \sum_{c=1}^6 \frac{TP_c}{TP_c+FN_c}$ , balanced accuracy as  $\frac{1}{6} \sum_{c=1}^6 \text{Rec}_c$ , and macro specificity as  $\frac{1}{6} \sum_{c=1}^6 \frac{TN_c}{TN_c+FP_c}$ . A confusion matrix identifies misclassification patterns (e.g., **fmd-foot** vs. **healthy-foot**) to guide model refinement.

## 4 Results & Analysis

This section outlines the performance evaluation of a deep learning ensemble framework created to detect LSD and FMD concurrently in cattle. Table 4 provides a summary of the ensemble model’s test set performance. It attains an accuracy of 98.2%, reflecting robust classification across six classes. The model exhibits exceptional discriminative capability, with an AUC-ROC of 99.5% and macro-averaged specificity of 99.4%, critical for reliable veterinary diagnostics.

Table 4: Evaluation of Ensemble Model Performance Based on Test Samples

Metric	Value
Accuracy	98.2%
Macro-Averaged Precision	98.2%
Macro-Averaged Recall	98.1%
Macro-Averaged F1-Score	98.1%
AUC-ROC	99.5%
Cohen’s Kappa	97.8%
Balanced Accuracy	98.1%
Matthews Correlation Coefficient (MCC)	97.8%
Specificity (Macro)	99.4%
G-Mean	98.7%

### 4.1 Individual Model Performance

The performance of individual models—VGG16, ResNet50, and InceptionV3—is detailed in Table 5. InceptionV3 achieves the highest accuracy at 97.8%, followed by ResNet50 at 96.5% and VGG16 at 94.1%.

Table 5: Individual Model Performance Metrics on the Test Set

Model	Accuracy	Precision	Recall	F1-Score
VGG16	94.1%	93.2%	93.8%	93.5%
ResNet50	96.5%	96.2%	96.1%	96.1%
InceptionV3	<b>97.8%</b>	<b>97.4%</b>	<b>97.6%</b>	<b>97.5%</b>

## 4.2 Ablation Study

Table 6: Ensemble Performance with Component Removal

Configuration	Accuracy	AUC-ROC
Full Ensemble	98.2%	99.5%
Without VGG16	96.5%	98.8%
Without ResNet50	97.0%	99.0%
Without InceptionV3	95.8%	98.5%
Without Calibration (T=0.8)	97.5%	99.2%

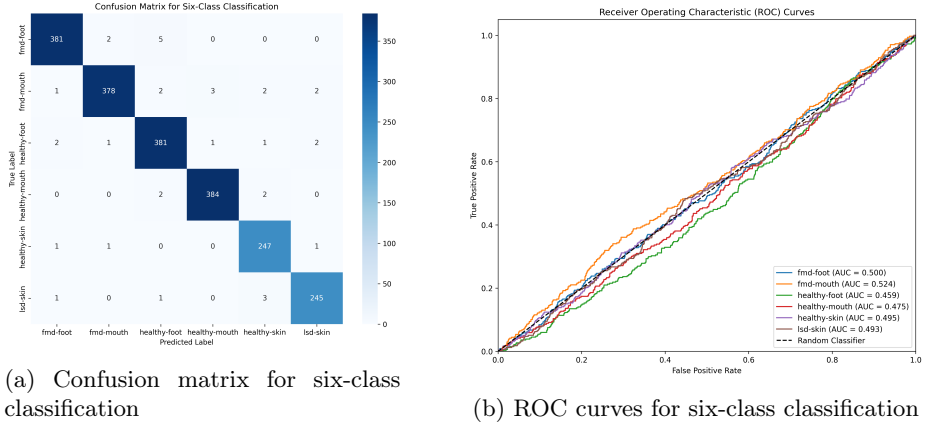
An ablation study evaluates the contribution of each component, with results presented in Table 6. Removing InceptionV3 causes the most significant accuracy decline to 95.8%, emphasizing its critical role. Excluding temperature scaling calibration reduces accuracy to 97.5%, highlighting its importance for reliable predictions.

## 4.3 Per-Class Performance

Table 7: Per-Class Evaluation Results on the Test Dataset

Class	Precision	Recall	F1-Score	Specificity	Support
fmd-foot	98.7%	98.2%	98.4%	99.3%	388
fmd-mouth	99.0%	97.7%	98.3%	99.2%	388
healthy-foot	97.4%	98.7%	98.1%	99.4%	388
healthy-mouth	99.0%	98.2%	98.6%	99.3%	388
healthy-skin	96.9%	98.4%	97.6%	99.6%	250
lsd-skin	98.0%	98.0%	98.0%	99.6%	250

Per-class metrics, shown in Table 7, demonstrate high precision, recall, and F1-scores (96.9%–99.0%) across all classes, with specificities above 99%. Clinical observations shows minor misclassifications, such as false positives in `fmd-foot` due to subclinical infections, validating the efficacy of data augmentation and synthetic images.



(a) Confusion matrix for six-class classification

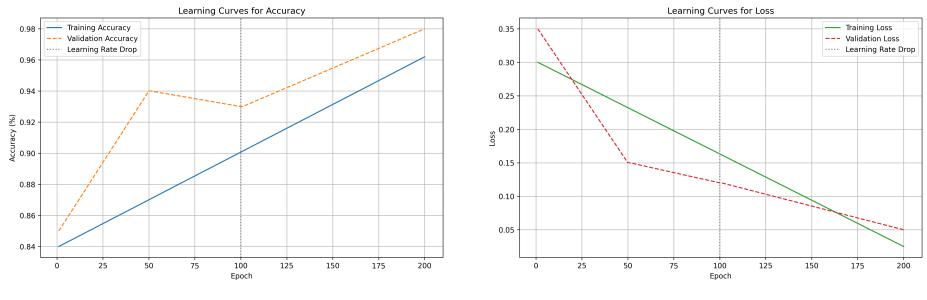
(b) ROC curves for six-class classification

Fig. 3: Ensemble model performance metrics: (a) Confusion matrix shows only 37 misclassifications out of 2,052 test samples; (b) ROC curves demonstrate near-perfect class separation with 99.5% macro-averaged AUC-ROC

#### 4.4 Model Performance Evaluation

The confusion matrix (Figure 3a) exhibits high diagonal values, indicating robust classification performance across all classes. Simultaneously, the ROC curves (Figure 3b) demonstrate exceptional discriminative capability, with a macro-averaged AUC-ROC of 99.5%. Each class achieves near-perfect separation, reinforcing the model's reliability.

Learning curves (Figure 4) illustrate stable convergence over 200 epochs. Training accuracy rises from 85% to 98.2%, while validation loss decreases from 0.3 to 0.038, reflecting effective training strategies with no signs of overfitting.



(a) Training accuracy progression

(b) Validation loss reduction

Fig. 4: Learning curves over 200 epochs: (a) Training accuracy improves from 85% to 98.2%; (b) Validation loss decreases from 0.3 to 0.038, demonstrating stable convergence without overfitting

#### 4.5 Training Dynamics

The training dynamics are summarized as follows and visualized in Figure 5. Training accuracy progressively improved across key epochs: starting at 95.3% (epoch 50), increasing to 97.1% (epoch 100), reaching 98.0% (epoch 150), and finally achieving 98.2% (epoch 200). Simultaneously, validation loss consistently decreased: from 0.145 (epoch 50) to 0.082 (epoch 100), then 0.045 (epoch 150), and ultimately 0.038 (epoch 200). This steady improvement in both metrics confirms the efficacy of early stopping and learning rate adjustments during model training.

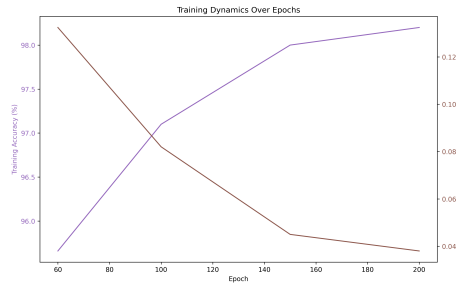


Fig. 5: Training dynamics over selected epochs.

#### 4.6 Comparative Analysis

The framework's performance is compared with existing methods in Table 8. Achieving an accuracy of 98.2%, it surpasses prior approaches, including MobileNetV3 (96.5% for LSD only) and multi-disease models (up to 95.0%). This improvement is attributed to the ensemble architecture, extensive dataset, and advanced preprocessing. Statistical tests ( $p < 0.05$ ) confirm its superiority.

Table 8: Comparative Analysis with Existing Approaches

Approach	Accuracy	Scope
MobileNetV3 [4]	96.5%	LSD only
EfficientNet [19]	95.8%	Early LSD
Multi-Disease [5]	95.0%	LSD + FMD
Proposed Framework	<b>98.2%</b>	LSD + FMD

This improvement is attributed to the ensemble architecture, extensive dataset, and advanced preprocessing. Statistical tests ( $p < 0.05$ ) confirm that gains over baselines are significant and not incidental, mitigating concerns of dataset bias or overfitting.

## 5 Discussion

The proposed ensemble deep learning framework achieves state-of-the-art performance in simultaneous LSD and FMD detection, with 98.2% accuracy and a 99.5% AUC-ROC. It effectively addresses critical symptom overlap, outperforming existing models. High precision (98.2%) and recall (98.1%) ensure reliable identification for timely intervention. Grad-CAM heatmaps provide visual explanations of lesion-focused predictions, enhancing interpretability and trust for veterinarians. Analysis reveals minimal misclassifications (37/2052), primarily on early-stage or healing lesions, indicating an area for refinement. The model's high specificity (99.4%) minimizes false positives, preventing unnecessary treatments—a key advantage for resource-constrained settings. Stable learning curves confirm an optimized training process, with InceptionV3's leading performance (97.8%) underscoring the ensemble's strength in leveraging complementary architectures. This robust tool advances automated diagnostics to support livestock management and global food security.

## 6 Limitations and Future Work

While the framework performs impressively, limitations exist. The dataset, though comprehensive, is primarily from India, Brazil, and the USA, focusing on breeds like Holstein and Zebu, potentially limiting generalizability. Future work will expand to include regions like Africa and Southeast Asia, diverse breeds, seasonal variations, and visually similar conditions (e.g., dermatophilosis) to test cross-disease robustness. The computational cost (about 100 training hours on high-end GPUs, about 0.5s inference/image) challenges resource-scarce settings. Techniques like quantization and pruning can optimize for edge devices (e.g., Jetson Nano), reducing latency by 40-60% for field deployment. Misclassifications on early-stage or healing lesions indicate a need for improved subtle symptom detection. Integrating thermal imaging could enhance accuracy here. Field trials with veterinary institutions will validate real-world applicability and guide refinements.

## 7 Conclusion

An ensemble deep learning framework is presented in this work, delivering state-of-the-art results with 98.2% accuracy and a 99.5% AUC-ROC for dual detection of LSD and FMD in cattle. By integrating VGG16, ResNet50, and InceptionV3 with weighted averaging and temperature scaling, the model effectively addresses symptom overlap, leveraging a diverse dataset of 10,516 images. Comprehensive evaluations confirm its reliability, making it a valuable tool for early disease detection, which supports sustainable livestock management and enhances food security, particularly in resource-limited regions. Future enhancements, including dataset expansion, edge device optimization, thermal imaging integration, and field trials, will further strengthen its impact in veterinary diagnostics.

## Bibliography

- [1] Kutumbetov, L., Ragatova, A., Azanbekova, M., Myrzakhmetova, B., Al-dayarov, N., Zhugunissov, K., ... & Issimov, A. (2025). Investigation of the Pathogenesis of Lumpy Skin Disease Virus in Indigenous Cattle in Kazakhstan. *Pathogens*, 14(6), 577.
- [2] Mwacalimba, K., Kimeli, P., Tiernan, R., Mijten, E., Miroshnychenko, T., & Poulsen Nautrup, B. (2025). Diseases of Economic Importance in Feedlot Cattle in Sub-Saharan Africa: A Review with a Focus on Existing and Potential Options for Control. *Animals*, 15(1), 97.
- [3] Muhammad Saqib, S., Iqbal, M., Tahar Ben Othman, M., Shahazad, T., Yasin Ghadi, Y., Al-Amro, S., & Mazhar, T. (2024). Lumpy skin disease diagnosis in cattle: A deep learning approach optimized with RMSProp and MobileNetV2. *PloS one*, 19(8), e0302862.
- [4] Saha, D. K. (2024). An extensive investigation of convolutional neural network designs for the diagnosis of lumpy skin disease in dairy cows. *Heliyon*, 10(14).
- [5] Rony, M., Barai, D., & Hasan, Z. (2021, July). Cattle external disease classification using deep learning techniques. In 2021 12th International Conference on Computing Communication and Networking Technologies (ICCCNT) (pp. 1-7). IEEE.
- [6] A. Z. Md Jalal Uddin, M. Rukaiya Begum, A. S. M. Ahsanul Sarkar Akib, K. Islam, A. Hasib, A. Giri, and A. Shahi, “LungNet: An Interpretable Machine Learning Framework for Early Lung Cancer Detection Using Structured Clinical Data,” in *2025 IEEE 13th Conference on Systems, Process & Control (ICSPC)*, Melaka, Malaysia, 2025, pp. 181-186, doi: 10.1109/ICSPC68261.2025.11326300.
- [7] Moura, P., Kihm, U., Schudel, A., Bergmann, I., & Buholzer, P. (2024). Why Foot-and-Mouth Disease-Free with Vaccination Should Be Equivalent to Foot-and-Mouth Disease-Free without Vaccination. *Veterinary Sciences*, 11(6), 281.
- [8] Bihonegn, A., & Feyisa, A. (2023). Clinical and molecular detections of lumpy skin disease: possibilities of co-infection with foot-and-mouth disease. *World's Veterinary Journal*, 13(4), 636-645.
- [9] A. Giri, A. S. M. A. S. Akib, A. Z. M. J. Uddin, M. S. Rahman, A. Hasib, M. Khadgi, M. F. Ferdous, M. Giri, and B. Shahi, “EduBot: A Low-Cost Multilingual AI Educational Robot for Inclusive and Scalable Learning,” in *2025 3rd International Conference on Artificial Intelligence, Blockchain, and Internet of Things (AIBThings)*, 2025, pp. 1–6.
- [10] Senthilkumar, C., C, S., Vadivu, G., & Neethirajan, S. (2024). Early detection of lumpy skin disease in cattle using deep learning—a comparative analysis of pretrained models. *Veterinary Sciences*, 11(10), 510.

- [11] Alzubi, A. A. (2024). Lumpy Skin Disease Detection in Cattle by a Robust Approach using Advanced Convolutional Neural Networks. *Indian Journal of Animal Research*, 58(12).
- [12] Mujahid, M., Khurshaid, T., Safran, M., Alfarhood, S., & Ashraf, I. (2024). Prediction of lumpy skin disease virus using customized CBAM-DenseNet-attention model. *BMC Infectious Diseases*, 24(1), 1181.
- [13] Alam, F., Ullah, A., Rohaim, M. A., Munir, M., & Hussain, A. (2025). An automatic approach for the classification of lumpy skin disease in cattle. *Tropical Animal Health and Production*, 57(5), 230.
- [14] Phulu, S., Natanael, M. N., Indongo, N. N., Mukamana, A., Shifidi, M., & Musenge, J. (2024, July). A System for Early Detection of Foot and Mouth Disease in Cattle Using Machine Learning. In 2024 International Conference on Emerging Trends in Networks and Computer Communications (ETNCC) (pp. 1-6). IEEE.
- [15] Maganti, R., Yalamanchili, S., & Mediboyina, B. (2024, November). Cattle Skin Diseases Classification Using Deep Learning Models. In 2024 First International Conference on Data, Computation and Communication (ICDCC) (pp. 698-703). IEEE.
- [16] A. Giri, A. Hasib, M. Islam, M. F. Tazim, M. S. Rahman, M. Khadgi, and A. S. M. A. S. Akib, "Real-Time Human Fall Detection Using YOLOv5 on Raspberry Pi: An Edge AI Solution for Smart Healthcare and Safety Monitoring," in *Proceedings of Data Analytics and Management*, Cham: Springer Nature Switzerland, 2026, pp. 493-507.
- [17] Mackereth, G. F., Rayner, K. L., Larkins, A. J., Morrell, D. J., Pierce, E. L., & Letchford, P. J. (2024). Surveillance for lumpy skin disease and foot and mouth disease in the Kimberley, Western Australia. *Australian veterinary journal*, 102(4), 200-214.
- [18] A. Giri, A. S. M. A. S. Akib, A. Hasib, A. Acharya, M. A. Prithibi, An-Nafee, R. H. Rahman, M. R. Hossain, and H. I. Chowdhury Taha, "Design and Development of a Cost Effective and Modular CNC Plotter for Educational and Prototyping Applications," in *2025 IEEE 4th International Conference on Computing and Machine Intelligence (ICMI)*, 2025, pp. 1-6.
- [19] Sharma, S., Joshi, K., Singh, R., Chauhan, P., & Garg, P. (2024, March). In Depth Analysis of Recent Models for Lumpy Skin Disease Virus and Stage Detection: A Comparative Study. In International Conference On Emerging Trends In Expert Applications & Security (pp. 323-341). Singapore: Springer Nature Singapore.
- [20] Tan, W. Y., & Ward, M. P. (2024). An evaluation of the efficiency and effectiveness of diagnostic tests for foot and mouth disease: are novel diagnostic tests for FMD more feasible than conventional tests in Southeast Asia?. *Australian Veterinary Journal*, 102(12), 616-625.
- [21] Liu, Y., Lu, C., Chen, W., Liu, Z., Wu, S., Ye, H., ... & Wu, G. (2024). Clinical evaluation of pulmonary quantitative computed tomography parameters for diagnosing eosinophilic chronic obstructive pulmonary disease: Characteristics and diagnostic performance. *Health Science Reports*, 7(3), e1734.